Case Studies in Construction Materials 17 (2022) e01564

Contents lists available at ScienceDirect

Case Studies in Construction Materials

journal homepage: www.elsevier.com/locate/cscm

Experimental evaluation of natural hydraulic lime renders with nanoclay and nanolime to protect raw earth building surfaces

Francesca Stazi [a,*], Nicola Pierandrei [a], Costanzo Di Perna [b], Francesca Tittarelli [a]

[a] Department of Materials, Environmental Sciences and Urban Planning (SIMAU), Università Politecnica delle Marche, Italy
[b] Department of Industrial Engineering and Mathematical Sciences (DIISM), Università Politecnica delle Marche, Italy

ARTICLE INFO

Keywords:
Natural hydraulic lime
Earth
Nanoclay
Nanolime
Renders

ABSTRACT

In this study Natural Hydraulic Lime (NHL) was combined with clay and lime, the main cementitious materials used in ancient buildings, to develop a new render more suitable for applications on raw earth substrates. Nanoclay and nanolime have been separately added to a commercial NHL-based ready-mixed powder. Pure and nano-additivated NHL renders have been compared in terms of microstructure (by SEM and mercury porosimetry), mechanical performance (by dynamic elastic modulus, flexural and compressive strength tests), adhesion to the substrate (by shear strength and pull-off tests), erosion resistance (by pressure spray test), and thermo-hygrometric performance (by water absorption and thermal conductivity tests). The obtained results demonstrate that both nanoparticles increase the water absorption and decrease the mechanical properties of the render but enhance the adhesion with the earthen support and the protection against water erosion. Among the two nanoparticles, the addition of nanoclay was found to be preferable since it gives to the render the highest mechanical compatibility with the underlying layer and the best durability against erosion.

1. Introduction

Hydraulic lime, intended as a mix of lime and pozzolan set through hydration, has been used as a binding material for mortar production since ancient times, especially in humid areas with a high availability of limestone naturally containing clay impurities [1]. Between the 18th and 19th centuries, the field of hydraulic binders evolved with the production of NHL, obtained through a rapid hydration process by burning argillaceous or siliceous limestones, below the sintering point (at temperatures of 850–1000 °C), and the subsequent reduction to powder by slaking [2,3].

With the advent of Portland cement in the 19th century, NHLs production strongly decreased because the harder compressive strengths and water resistance of Portland cement were considered superior qualities. However, in recent years, cement-free NHL based mortars, have gained a renewed interest for applications in masonry bricklaying, internal plastering, and external rendering for different reasons. Compared to cement-based mortars, they have a lower environmental impact owing to reduced burning temperature. Moreover, they show a higher compatibility with historic masonries or raw earth surfaces because they have a greater ability to exchange water vapor thus preventing moisture condensation and because they present thermal expansion and mechanical elasticity values closer to the supporting material, thus allowing the accommodation of movements [3].

* Corresponding author.
E-mail addresses: f.stazi@univpm.it (F. Stazi), nicola.pierandrei@gmail.com (N. Pierandrei), c.diperna@univpm.it (C. Di Perna), f.tittarelli@univpm.it (F. Tittarelli).

https://doi.org/10.1016/j.cscm.2022.e01564
Received 1 April 2022; Received in revised form 20 September 2022; Accepted 11 October 2022
Available online 13 October 2022

In contrast to non-hydraulic limes, which harden by reaction with carbon dioxide in the air, hydraulic limes are characterized by the ability to harden with water and under high humidity conditions [4] as well as by faster and higher achievement of mechanical strength [5]. They also have the ability to improve their performance over time; when exposed to air, they react with atmospheric carbon dioxide by carbonation thus completing the hardening process [2], and behaving as CO_2 capturing materials. Moreover, because the carbonation process is long-lasting, they achieve higher strength in the long term than in the early stage, ensuring durable mechanical performance.

Owing to these advantages, NHL was successfully used in raw earth materials and blocks as stabilizer [6] and as binder in eco-friendly cement-free mortars. Moreover, it is increasingly used as a sacrificial breathable surface for the restoration and protection of walls [7] with damp and salt deposits and as a viable alternative to earthen mortars for plastering and rendering of raw earth walls of different types (adobe, cob, extruded bricks, rammed earth, and compressed earth blocks). Moreover, a recent use of NHL-based mortars concerns their application on the surfaces of extruded earthen claddings placed externally and internally in wooden panels of lightweight timber framed buildings [8] (Fig. 1). These claddings, which are made of unbaked and extruded earth blocks, are secured to external fir boards through metal anchors [9].

The literature on NHL rendering and plastering mortars mainly relates to the mix design optimization, and to the exploration of the effects of additives on the long-term performance of the final products.

Research on the mix design choice mainly considers the binder-to-sand ratio, water-to-binder ratio, sizes/packing density of aggregates and type of binder, all of which are found to play an important role in the mechanical and physical performance of NHL-based products [2,5]. This encouraged the proposal of a comprehensive framework to support the multiparametric mix design of NHL mortars [3]. Other authors, focusing on premixed mortars, stressed the different behavior due to unequal underlying substrate and curing conditions [10].

As far the influence of additives is concerned, several studies addressed different optimization purposes of hydraulic mortars: for waterproofing, for example using siloxane [11] or natural herbs [12]); for water retainment, for example with cellulose ethers additions [13]; to enhance the compatibility between historic masonries and restoration materials, for instance through siliceous sand and crushed brick [14]; to optimize the sound absorption through lightweight pumice aggregates [15]; to increase the mechanical performance and simultaneously tailor the water adsorption through ceramic residues [16] and waste graphite powder [17].

Formulations of NHL with expanded glass aggregates have been demonstrated to enhance the depolluting abilities of NHL mortars [18]. The addition of metakaolin to NHL mortars has been found to improve its strength characteristics especially under humid curing conditions but the pozzolanic compounds showed some instability with ageing determining a decrease of strength [19].

Few studies have suggested the adoption of nanotechnology to enhance natural hydraulic lime mortars. Among them, rather recent studies addressed the incorporation if graphene oxide in NHL mortars achieving a slight improvement of mechanical and physical characteristics [20]. The addition of nano-SiO_2 (2–3% by weight) has given an improvement of the mechanical properties, durability and compatibility with the masonry [21,22]. The addition of TiO_2 (3% by weight) has been found to: enhance the mortar-masonry compatibility, increase the elasticity modulus as well as humidity retention and, consequently, improve the adhesive capacity [23] and antifungal properties [24]. The addition of nano-TiO_2 and perlite to lime-metakaolin mortars has been demonstrated to lower the structure density with a decrease in mechanical properties but, conversely, an enhancement of salt decay resistance and thermal insulating properties [25]. The addition of nanofibers (for example cellulose fibers) to NHL has been found to have a positive effect on water resistance and render-support compatibility, but also to reduce the mechanical strength [26]. Moreover, most additions have been demonstrated to induce changes in the color and texture of hardened NHL pastes or mortars, making them unsuitable for heritage buildings.

Nanolime and nanoclay were selected in this study for their morphological and color compatibility with historic and earthy-based substrates and for their proven ability to provide hosting materials with enhanced mechanical properties. Indeed, nanoclay has been demonstrated to provide improved performance in terms of tensile strength and reduced microcracks in cement-based materials [27,28] and also to guarantee effective protection for highly porous stones and marbles [29]. Similarly, nanolimes have been shown to confer long-lasting antibacterial effects with promising applications in the cultural heritage field [30], and to increase both mechanical

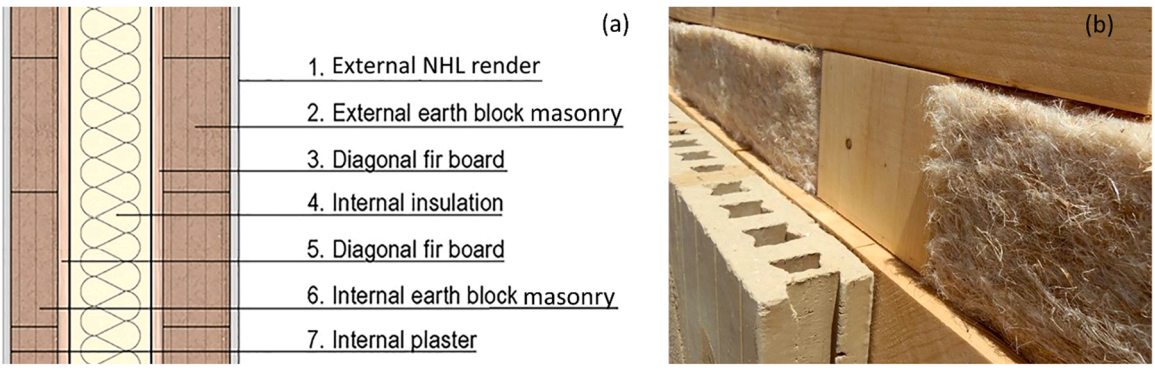

Fig. 1. Application of Natural Hydraulic Lime (NHL) renders on eco-friendly earthen building envelopes with timber-framed lightweight structure and hemp insulation: (a) schematic section of the wall; (b) image of the wall.

and water resistance properties when applied to lime mortar substrates [31,32]. However, to the best of the authors' knowledge, no studies have addressed the adoption of nanoclay or nanolime in natural hydraulic lime renderings. Their contribution to the mechanical, and thermophysical performance of NLH is still not fully understood. Moreover, the durability of NHL respect the destructive action of weathering has been addressed for mortar joints in masonries bricklaying [10,33,34] while rarer are the studies on surface rendering materials. This latter issue is becoming increasingly important in light of the recent increasing occurrence of extreme rainfall events due to the well-known worldwide climate change. More studies on the development of natural cement-free rendering solutions, compatible with buildings of historical interest and earthen substrates that are able to protect external surfaces against weathering are needed.

Therefore, the aim of this study was to contribute to fill the identified open issues by evaluating the effectiveness of the addition of nanolime or nanoclay to Natural Hydraulic Lime (NHL) renderings, to protect undelaying raw earth substrates. To this end, pure and additivated specimens were compared in terms of microstructure by SEM and mercury porosimetry, mechanical performance by dynamic elastic modulus, flexural and compressive strength, adhesion to the substrate by shear strength and pull-off tests, erosion resistance by pressure spray test, and thermo-hygrometric performance in terms of water absorption and thermal conductivity.

2. Materials

2.1. Rendering mortars formulation

A commercial ready-mixed powder, Kerakoll Biocalce, was used in the experimentation. According to the technical datasheet it contains 20% of pure NHL 3.5, 1–2.5% of ultra-thin pozzolanic additives, 2.5–10% of silica sand with two different grain size fractions (0.1–1 mm and 0.1–0.5 mm), and 50–75% of a medium sized powder (0–2.5 mm) of dolomitic limestone. The apparent density of the adopted ready-mixed powder is reported as 1.28 kg/dm^3. The binder is classified as NHL 3.5, (moderately hydraulic) according to EN 459–1:2015 [35], where the number stands for the minimum compressive strength at 28 days of hardening in N/mm^2. The more hydraulic the lime is, the faster it sets, and the higher its final strength. NHL 3.5 was selected because it is frequently used for external works and it is expected to be more 'breathable' and more flexible than NHL5.

The base mortar (CA) was obtained by adding the powder to clean water following the amounts suggested by the technical data sheet (25 kg of ready premixed powder in 5.1 l of water), corresponding to a water/lime ratio by weight of about 1.

The fresh mortar was then mixed manually with a trowel for 5 min, until a uniform mix. The consistency was determined using a flow table test according to EN 1015–3 obtaining a final flow value of 170 mm corresponding to a soft consistency. The apparent density of the dry hardened mortar was 1.6 kg/dm^3.

Two different nanoparticles were added separately to the base mortar: *nanoclay* and *nanolime.* The nanoparticles were added in an amount equal to 2% of the dry weight of premixed powder (Table 1).

In the case of *nanoclay* (CC), a commercial hydrophilic bentonite (Sigma-Aldrich) clay was used. According to the data sheet, it consists of ~ 1 nm thick aluminosilicate layers surface-substituted with metal cations and stacked in ~ 10 μm-sized multilayer stacks; the relative density is 2.400 g/cm^3.

The particles were previously added to the powder in dry state, and then clean water was incorporated through a trowel for 5 min

In the case of *nanolime* (CL), only nanolime suspensions in alcohols were commercially available. In this case commercial colloidal nano-particles of lime hydrate suspended in ethanol, with a concentration of 25 g/l, typically adopted for stone and plaster consolidation, were used (CaLoSil, IBZ-Salzchemie & Co.KG). According to the data sheet, the particles sizes are between 50 nm and 250 nm with an average value of 150 nm. Ethanol was previously separated by a simple distillation process by heating the solution at T = 78 ± 2 °C. A small ethanol portion (4% of dry lime weight) was maintained to avoid the onset of the carbonation process of nanolime in contact with air and to favor the particle dispersion through mechanical mixing. Subsequently, the components were manually mixed with water and the render was smoothened with a trowel.

The final mixes are reported in Table 1.

2.2. Rendering mortar specimens

Different types of rendering mortar specimens were realized:

- Specimens applied to walls or to single clay blocks.

Table 1
Typologies and composition of the different render mixes.

N°	Name	Composition	NHL (g)[a]	(%)[b]	Nanoclay (g)[a]	(%)[b]	Nanolime (g)[a]	(%)[b]	Ethanol (g)[a]	(%)[b]
1	CA	Natural hydraulic lime (NHL)	1000	79	–	–	–	–	–	–
2	CC	NHL + nanoclay	1000	77	20	2	–	–	–	–
3	CL	NHL + nanolime	1000	77	–	–	20	2	40	4

[a] Dry mass.
[b] Percentage by mass of NHL.

- Specimens with sizes according to the test standards, not applied to the support.

The first group of specimens consisted of a uniform layer of 20 mm thick as suggested by EN 1015-12:2016 [36] and also by [37] and [38]. The undelaying application area of the wall was cleaned with a brush and wetted with a water spray. The renders were then applied and smoothed to the wall with a trowel and shaped with the aid of steel molds. The application envisaged a single layer of mortar as suggested by the manufacturer.

The specimens belonging to the second group were produced by casting and compacting mortar in standard steel molds.

All the renders (either single specimens or those applied on earthen walls) were covered with polyethylene films in the first week of curing and subsequently left 21 days under laboratory conditions (T = 20 °C ± 3 °C; RH = 60 ± 5%) by removing the plastic protections.

The specimen dimensions and numbers are summarized in Table 2.

2.3. Earth walls substrate

Four earth walls were built as substrate for applying the renders, equal to those used for external massive claddings in timber-framed buildings (Fig. 1). Therefore, masonry with unfired and extruded raw earth blocks was selected. The block composition was based on a matrix of clayey soil (70%) and wooden fibers (30%) as natural stabilizers. Each earth block had nominal dimensions of 215 mm × 230 mm x 115 mm. Laterally, the dovetail joints served as a guide for aligning the blocks and ensuring their mechanical connection.

The dimensions of the 4 walls were 45 cm× 70 cm× 10 cm. Their realization involved the following steps: (i) clay was mixed with water at a ratio of 2:1; (ii) the lateral and lower surfaces of each block were uniformly wetted in this clay-based mortar; and (iii) each block was layed by sliding it vertically along the dovetail joints.

The walls were cured for three months in a controlled laboratory environment (T = 20 °C ± 3 °C; RH = 60 ± 5%).

3. Experimental methods

3.1. Render characterization

Mortar characterization analyses were conducted by SEM and mercury porosimetry test.

SEM was used to evaluate the microstructure of the samples (Instrument Model: VEGA with accelerating voltage from 200 V to 30 kV and resolution of 3 nm at 30 kV). Three samples of 10 mm × 10 mm× 10 mm were analyzed for each formulation. They were obtained from the fragments of the specimens that have previously been subjected to mechanical tests. To prevent the accumulation of electrostatic charges at the surface, the samples were coated with an ultrathin coating of gold by high-vacuum evaporation.

Mercury porosimetry analyses were used to obtain the percentage of open porosity and dimensional distribution of the pores of the samples immersed in a mercury bath with increasing pressure (Instrument Pascal 140/240, ThermoFisher). Three samples of 10 mm × 10 mm × 10 mm obtained from the fragments of the specimens that have previously been subjected to mechanical tests, were analysed for each formulation. The Washburn equation [39] was used to relate the applied pressure to the pore radius. A contact angle of 135°, a Hg surface tension of 0.56 N/m and a pressure ranging from 0 to 200 MPa were adopted.

3.2. Render mechanical strength and adhesion to the substrate

The mechanical performance of the renders and their adhesion to the substrate were evaluated through mechanical strength tests (dynamic elastic modulus, flexural strength, and compressive strength) and shear/pull off test. For each mechanical test, the experiments involved the casting of three specimens (40 mm × 40 mm × 160 mm) in steel molds.

The dynamic elastic modulus E_d (N/mm^2) was evaluated through Pundit ultrasonic tester by measuring the wave propagation speed in the mortar specimens (Fig. 2a), according to EN 12504-4:2021 [40].

The flexural (Fig. 2b) *and compressive strengths* (Fig. 2c) were assessed through a 400 kN hydraulic press (Galdabini, Italy) according to EN 1015-11:2019 [41].

Table 2
Number and size of specimens (CA, CC, and CL) for each test.

	CA	CC	CL	Size
Scanning Electronic Microscopy (SEM)	3	3	3	10 mm × 10 mm× 10 mm
Mercury Porosimetry	3	3	3	10 mm x 10 mm x 10 mm
Compression Tests	3	3	3	40 mm x 40 mm x 160 mm
Shear Test	5	5	5	50 mm × 40 mm x 20 mm
Pull-off Test	5	5	5	d = 50 mm, t = 20 mm
Karsten Pipe Test	3	3	3	250 mm × 250 mm x 20 mm
Heat Flow Meter Test	3[a]	3[a]	3[a]	300 mm × 300 mm x 30 mm
Erosion Test	3[a]	3[a]	3[a]	250 mm × 250 mm x 20 mm

[a] Three different measurement points on one specimen.

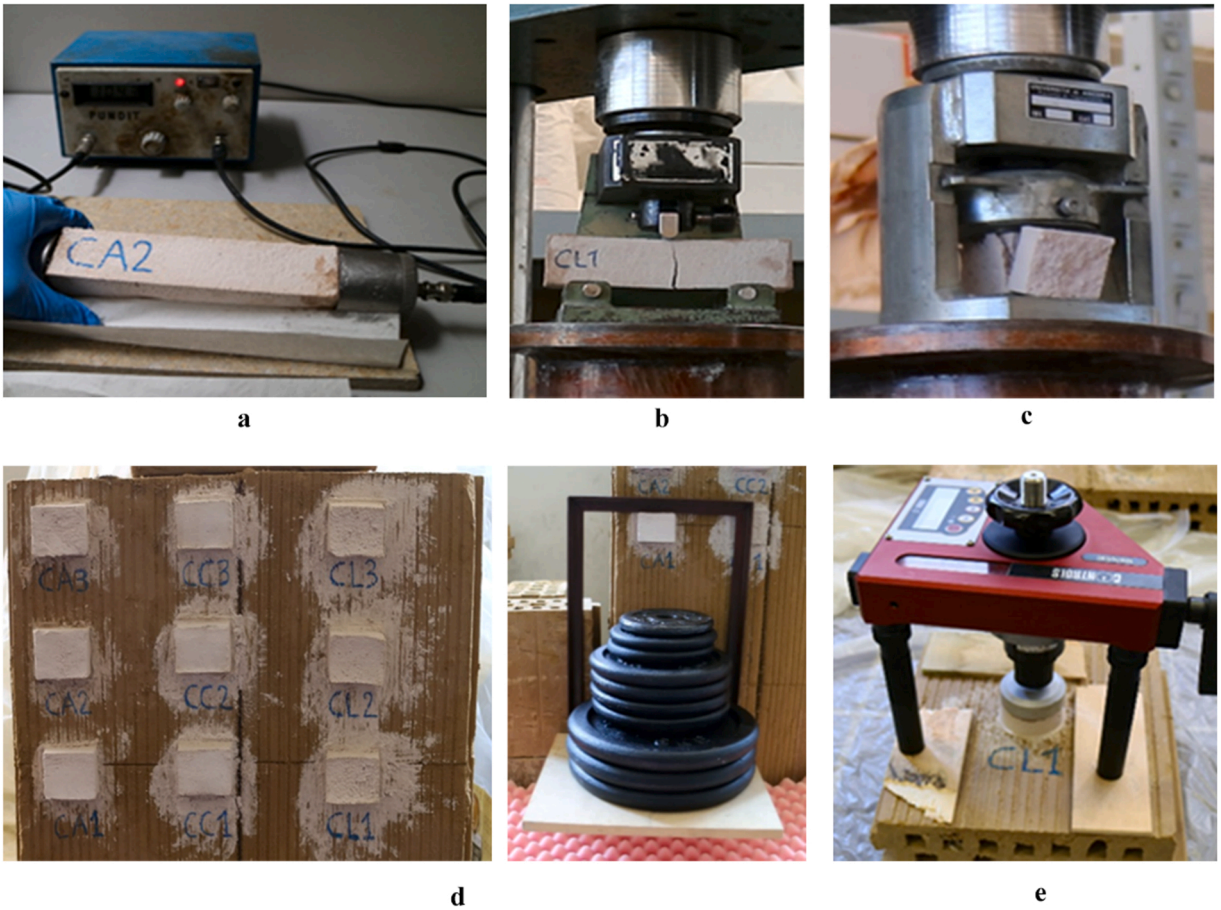

Fig. 2. Mechanical strength and adhesion tests details: a) Measurement of the wave propagation speed; b) Flexural test; c) Compressive test; d) Shear test; e) Pull off test.

To determine the flexural strength, a load was applied at a uniform rate of 10 N/s providing the failure occurrence within a period of 30–90 s.

The compressive strength was measured by applying an increasing load at a speed of 100 N/s (according to Annex B, Category *CS II*) until failure on specimens with nominal cross section area of 1600 mm^2. The strength of each specimen was recorded at the nearest 0.05 N/mm^2. The category of each mortar was classified according to EN 998-1:2016 [42] by averaging the values of the three specimens and approximating the results to the nearest 0.1 N/mm^2.

The adhesive strength was evaluated through shear test according to the procedure proposed by Hamard et al. [37]. For each render formulation, 5 specimens (50 mm × 40 mm × 20 mm) were applied on the wall panels for a total of 15 specimens (Fig. 2d). After curing, the specimens were loaded until failure by increments of 0.5 kg applied for 15 s. Some adaptations were applied to the wooden loading device proposed by Hamard, as the insertion of a metal sheet frame, owing to higher loads. Once the failure mass is recorded, the average shear strength (τ_{max}, N/mm^2) was calculated as follows:

$$\tau_{max} = \frac{m_f \cdot g}{S} \tag{1}$$

where m_f is the failure mass (kg), g is the gravitational acceleration = 9.81 m/s^2, and S is the specimen surface area (mm^2).

The adhesive strength was also evaluated using a pull-off test (Fig. 2e) according to EN 1015-12:2016 [36] with the aid of a Pull-off tester Controls 58-C0215. Five specimens were prepared for each render formulation, for a total of 15 specimens, and were applied to the unbaked clay blocks. The diameter of the renders was 50 mm, and the thickness was 20 mm. After curing, the pull-head was glued centrally on the test area. A load without shock was applied at a uniform rate of 0.011 N/mm^2s, so that failure occurred between 20 and 60 s.

Individual adhesive strengths were recorded at the nearest 0.05 N/mm^2. The adhesive strength was calculated as the mean value of the individual values of the five specimens for each type of render mortar to the nearest 0.1 N/mm^2.

3.3. Thermo-hygrometric tests

Thermo-hygrometric tests included water absorption and thermal conductivity tests.

Water absorption by capillarity was evaluated using the Karsten pipe method with a tool designed according to EN 16302:2013 [43] and referring to [44] for adaptations and simplifications. The Karsten pipe is a tube graduated to the 10^{th} of a millimeter provided, at the lower end, with an aperture of 500 mm^2 internal area. The pipe was sealed to the sample with mastic and then filled with water. The initial water column, 92 mm high, exerted a pressure of 900 Pa in the contact area between the pipe and specimen surface. The tests were carried out on three specimens, 250 mm × 250 mm × 20 mm in size, applied to the wall panels in raw earth. For each render formulation, the water absorption rate was evaluated at two test points, with readings of the reduction in the water level every minute for 15 min.

Thermal conductivity was evaluated using the heat flow meter method according to UNI EN 12664:2002 [45]. For each render formulation, one specimen was realized with dimensions of 300 mm × 300 mm × 30 mm for a total of three specimens. The samples were poured into steel molds. The test system (Fig. 3) was composed of a box of insulating material that was closed during the execution of the test to ensure an adiabatic internal environment. A unidirectional constant heat flow was generated by adopting a hot and cold plate connected to thermostatically controlled water baths at T = 25 °C and T = 15 °C, respectively. Temperature probes and flowmeters on both sides of the specimen were used to measure the thermal gradient and crossing heat flux in three different sample points and the final data were obtained as average values. Initially, the system was calibrated using a panel with known thermal conductivity. The test duration was 24 h for all the samples.

3.4. Erosion test

The aim of the test was to comparatively measure the durability of the rendering mortars as sacrificial surfaces under the worst conditions represented by the eventuality of eroded topcoat finishing. *Water erosion resistance* was evaluated using the pressure spray method (Fig. 4), according to the New Zealand Standard NZS 4298:2020 [46] and a previous study by our research group for adaptations and simplifications [38] also in consideration of the higher strength of the tested material respect to clay materials for which the standard is specifically focused. The test was carried out with a tool designed according to the standard on three specimens of size 250 mm × 250 mm × 20 mm, applied as in the current technique in a unique layer (20 mm thick) to the earthen wall panels. The test lasted for 60 min, and the erosion depth (D, mm) was measured every 15 min. The water jet was projected by a distance of 470 mm at a pressure of 50 kPa, simulating the accelerated aging by means of the action exerted by the wind-driven rain.

4. Results and discussions

The following subsections present the results of the experimental tests. The data are summarized in Table 3.

4.1. Render characterization

The *SEM* observations (Figs. 5–7) showed that in CA and CL, the microstructure was heterogeneous with flat hexagonal portlandite crystals, needle-like hydration products and aggregates. On the other hand, portlandite crystals were not present in CC, probably because of the pozzolanic reaction between clay and lime hydroxide, which also gave a more homogeneous and compact microstructure.

The addition of 2% of nanoclay (CC) created a denser microstructure than the reference CA because the nanoparticles filled the voids thanks also to the pozzolanic reaction. This result confirms the findings of Farzadnia et al. [47], who evaluated the properties and microstructure of cementitious mortars with different percentages of nanoclay. The authors highlighted that nanoclay addition led to a more homogeneous microstructure with enhanced properties owing to the consumption of portlandite in the cement matrix because of the pozzolanic reaction, even with swelling drawbacks.

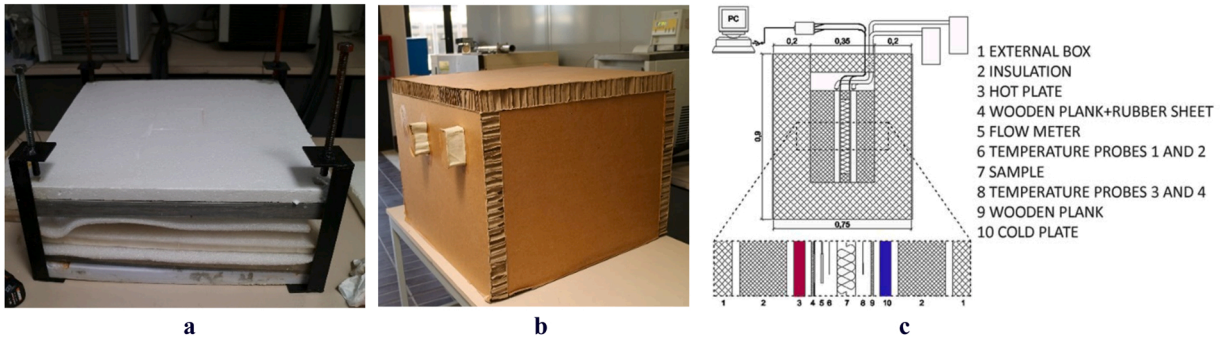

Fig. 3. Thermo-hygrometric test: a) combined stratigraphy including sample and hot/cold plates; b) insulated box; c) testing apparatus scheme.

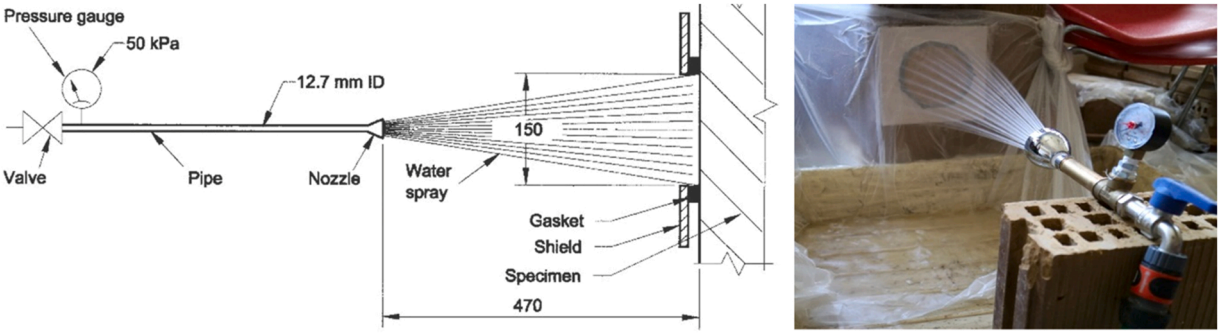

Fig. 4. Pressure spray erosion test details.

Table 3
Results obtained with the tests carried out on the different mortars.

Parameters	Mean values (standard deviation)			Tool/Standard
	CA	CC	CL	
Total open porosity (%)	39 (± 2)	24 (± 1)	36 (± 2)	Mercury Porosimeter
Average Pore diameter (μm)	0.195 (± 0.004)	0.372 (± 0.005)	0.192 (± 0.004)	
Dynamic elastic modulus E_d (N/mm^2)	3705 (± 24)	2440 (± 39)	2764 (± 46)	Pundit Ultrasonic test/
Flexural strength f (N/mm^2)	1.60 (± 0.22)	0.80 (± 0.08)	1.00 (± 0.22)	EN 12504-4:2021
Compressive strength σ (N/mm^2)	3.50 (± 0.29)	2.00 (± 0.10)	2.40 (± 0.04)	Hydraulic press/ EN 1015–11:2019
Shear strength τ_{max} (N/mm^2)	0.197 (± 0.01)	0.176 (± 0.01)	0.173 (± 0.01)	Shear test [37]
Pull off strength f_u (N/mm^2)	0.24 (± 0.01)	0.18 (± 0.01)	0.16 (± 0.01)	EN 1015-12:2016
Water absorption rate $C_{KB10min}$ (g/m^{2}s^{-1})	0.46 (± 0.04)	1.33 (± 0.01)	0.71 (± 0.04)	Karsten pipe method/ EN 16302:2013
Thermal conductivity λ (W/(mK))	0.10 (± 0.01)	0.11 (± 0.01)	0.11 (± 0.01)	Heat flow meter method/ UNI EN 12664:2002
Erosion rate D (mm)	3 (± 0.5)	0 (± 0.0)	2 (± 0.5)	Water erosion test/ NZS 4298:2020
Bulk density of the dry hardened mortar (kg/m^3)	1580 (± 16)	1704 (± 8)	1634 (± 15)	EN 1015–10

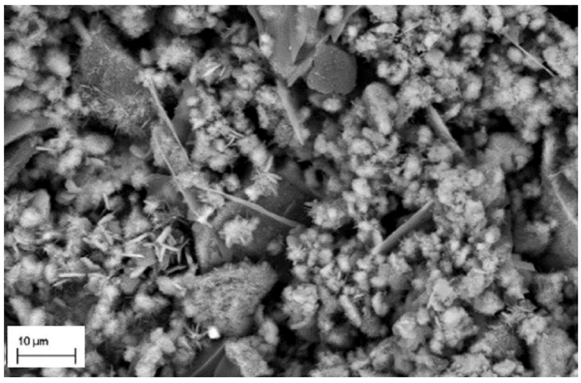

Fig. 5. SEM Observations: CA mortar.

Mercury porosimetry tests showed that the percentage of total open porosity decreased with the nanoparticles in the mixture (Fig. 8). The CA base render achieved a total open porosity value of 39% (Table 3). The most significant porosity decrease was obtained by CC formulation, with a value of 24%, confirming the SEM observations where CC microstructure appeared the most compact. CL instead recorded porosity values much closer to the reference render (both around 36%).

Even if nanoparticle addition decreased the total porosity of mortars, especially in nanoclay it slightly increased the average pore diameter, with values ranging from $d_{av} = 0.195$ μm for CA to $d_{av} = 0.372$ μm for CC.

The results were compared with the findings of other authors [14] relating to the restoration of a historic stone wall in Crete using a render mortar based on natural hydraulic lime. The cumulative volume (approximately 140 mm^3/g) as well as the open porosity value of 26%, recorded for the mortar in their work were very similar to the values obtained in the present work by CC (130 mm^3/g and 24%).

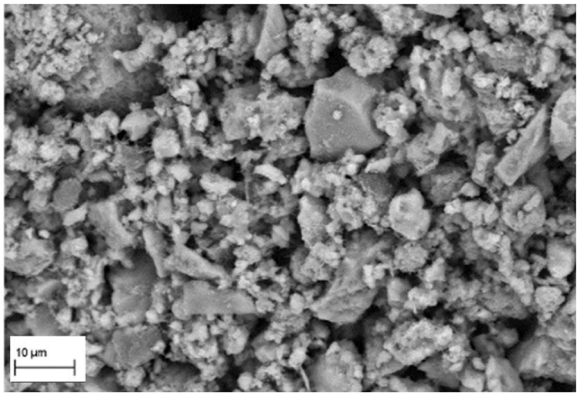

Fig. 6. SEM Observations: CC mortar.

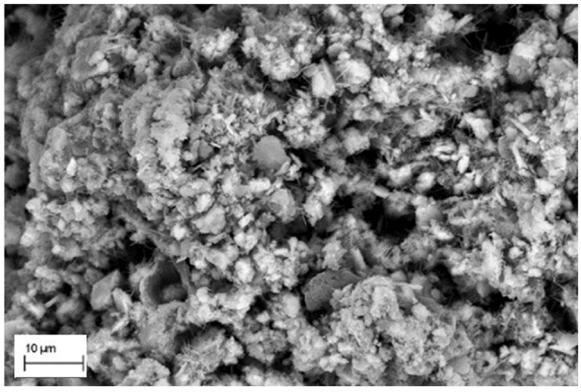

Fig. 7. SEM Observations: CL mortar.

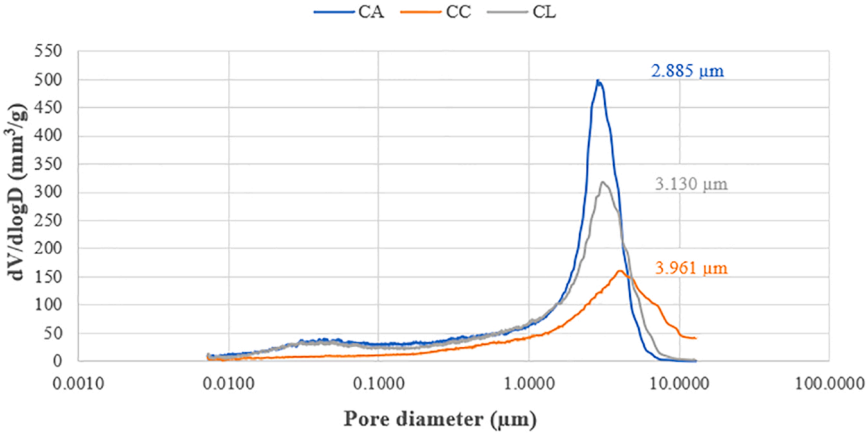

Fig. 8. Pore size distribution of different mortars.

Nanoparticles, as nanolime and nanoclay, are often introduced into cement-based materials to optimize the pore structure thanks to their physical action (filler action), which partially closes the porosity paths, and their ability to act as additional nucleation sites (nucleation effect) for the formation of new hydration products (C-S-H), accelerating the binder hydration [48], due to their high specific surface area [49–51]. Both these effects gave a closer and more compact structure, as SEM observations and the measured density values suggest. In addition, in the case of nanoclays, as reported above, the formation of secondary CSH produced by the pozzolanic reaction with calcium hydroxide, further contributed in giving a more closer and compact structure, as demonstrated for other types of formulations by [52–54].

However, unexpectedly, in the case of CC, even with a lower total open porosity, the average pore size was slightly increased. Due to its hydrophilic nature, the bentonite clay shows dramatic shrink and swell properties on hydration due to 2:1 layer arrangement of aluminosilicates [55]. The bentonite clay particles swell in the fresh mortar mix due to the absorption of water in their interlayer and release water and shrink during aging under low humidity, generating additional voids at the interface. These voids do not provide any resistance to the cracks development under loading and reduce the mechanical strength. As a matter of fact, pre-swelled bentonite slurry is also used as a pore forming agent in cement pastes [56].

4.2. *Render mechanical strength and adhesion*

The values of the Young's modulus ranged from 3705 N/mm^2 for CA to 2440 N/mm^2 for CC (Table 3). As specified by Hamard et al. [37] the best render is the one with the elastic modulus closest to (or lower than) that of the masonry; thus, the stresses are supported by the latter, thus preventing cracks or splits of the coating. Therefore, in the present work, the best render is that with 2% nanoclay additives because it has the lowest value and is closest to that of the raw earth masonry used as a support, as obtained in a previous study (E_d = 700 N/mm^2) [57].

Regarding the mechanical performance, the addition of the nanoparticles lowered both the *flexural and compressive strength* (Table 3) values of the render with respect to the reference render CA. However, all the renders remained within the CS II category (with regard to compression), falling in the range set by UNI EN 998-1:2016 [42]. In all cases, the nanoclayed CC mortar exhibited the lowest value; even if this sample showed the closest and most compact structure it was characterized by the presence of bigger pores than the other formulations (see Table 3) thus giving lower final strength values.

The results obtained from the adhesion tests showed that addition of nanoparticles did not produce a significant decrease in adhesion strength with the substrate, with values obtained by *shear tests* ranging from 0.197 N/mm^2 for CA to 0.173 N/mm^2 for CL (Table 3). In all the cases, a shear force equal to 10 times the render own weight was reached (a safety coefficient of 10 was assumed) [37].

Adhesion strength was also evaluated through the *pull-off* test, which recorded a slight decrease owing to the addition of

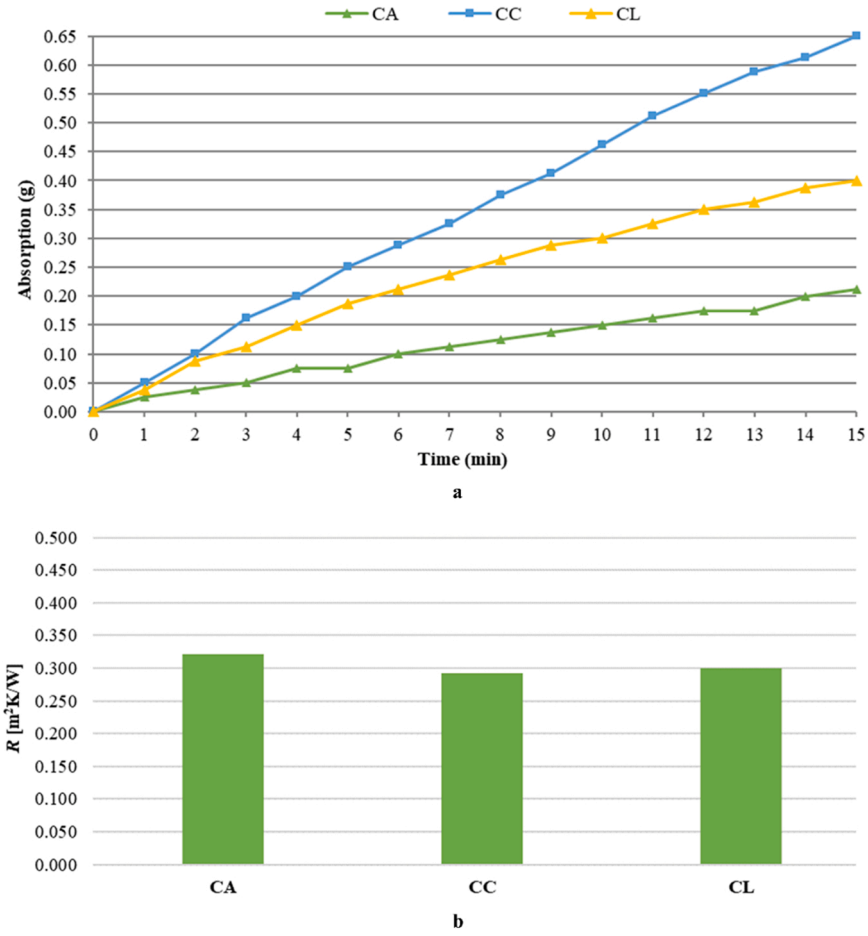

Fig. 9. Water absorption tests results (a) and samples thermal resistance (b).

nanoparticles. However, this performance reduction is negligible since, as suggested by UNI EN 1015-12:2016 [36], all the values can be approximated to 0.20 N/mm^2, satisfying in all cases the limit of 0.20 N/mm^2 set by UNI EN 998-1:2016 [42] (Table 3). For both the adhesion tests, the cracks occurred at the support-render interface. In summary, the renders showed similar behavior with regard to adhesion.

4.3. Thermo-hygrometric tests

The water absorption rates of the functionalized renders CC and CL (respectively of 1.33 g/m^{2}s^{-1} and 0.71 g/m^{2}s^{-1}) resulted greater than that of the reference render CA (equal to 0.46 g/m^{2}s^{-1}) (Fig. 9 and Table 3). The highest water absorption rate shown by CC is due to the larger average size of the pores, as demonstrated by the mercury porosimetry test and probably also to the ability of clay particles to adsorb water. Therefore this formulation is more prone to swelling due to the entrapment of water within its layers [14], increasing the probability of penetration of aggressive substances. The increase of water absorption with nanoclay has also been demonstrated for cement-based mortars [58].

For these mortars, an increase in water absorption, when the total open porosity increases and the dry density decreases, has been reported in the literature [59], confirming the results obtained in the present work.

The thermal conductivity of the renders with nanoparticles (Table 3) showed only a slight increase compared to the reference render, with a value of 0.10 W/(mK) for CA, 0.11 W/(mK) for CC and 0.11 W/(mK) for CL. However, the thermal resistance values (Fig. 9 b) remained within the limits set by the UNI EN 12664:2002 [45] ($R \geq 0.1$ m^{2}K/W).

In summary, the thermal conductivity test demonstrated that both nanoparticle additions resulted in only negligible reductions in thermal performance. This result is confirmed by other researchers' study [17], that found an increase of the thermal conductivity of a natural hydraulic lime (NHL) after the addition of 2% graphite powder.

This can be explained with the densification of the samples with additives (see Table 3) that are therefore subjected to increased conductive thermal flow.

4.4. Erosion test

The results of the erosion tests are shown in Fig. 10 and Table 3. This test is particularly important for conservative purposes because it characterizes the ability of the renders to protect the underlying supports. After an exposure to accelerated weathering for 60 min, the CC specimen showed the best outcome with no erosion, demonstrating excellent resistance. The other render types exhibited a low erosion depth. Although erosion occurred, the values were within the limits set by the NZS 4298: 2020 ($I = 1$).

In summary, the data demonstrated the best properties of the nanoclayed formulation compared to the others. High water absorbing materials are less prone to natural rain surface erosion. Moreover its low total open porosity and denser microstructure that the other coatings make its surface smoother and lesser liable to water erosion [60].

5. Conclusions

This study compares the effects of nanoclay and nanolime additions on the mechanical and durability properties of a commercial ready mixed render based on NHL used as protective layer for a raw earth masonry.

The outcomes can be summarized as follows:

- The nanoparticles improve the compatibility of the plaster with the earth masonry, thanks to the reduction of its dynamic elastic modulus up to 34%. This makes the stiffness of the protective layer closer to that of the substrate, so that stresses are supported by the latter during the service life, thus preventing cracks or splits of the render.
- Both nano-additions give to the NHL render an increased resistance against erosion due to atmospheric agents; the erosion depth decreased from 3 mm (in the reference formulation) to 2 mm with nanolime and to 0 mm with nanoclay. This is due to the nucleation effect of both nanofillers that gives a less porous and more compact structure to the render.
- An increase in the water absorption of the render is observed if both types of nanoparticles are added, with values more than doubled for nanoclay. This is due to the increase of the average pore size of the render in the presence of nanoparticles, even if with a decrease in the total porosity.
- The increase of the average pore size of the render with the addition of nanoparticles is responsible for the slight reduction of its mechanical properties in terms of flexural strength (−50% and −37% with nanoclay and nanolime additions, respectively), compression strength (−40% and −30% for nanoclay and nanolime additions, respectively) and adhesion to the wall (−10% reduction in shear strength for suspended loads with both nanoparticles).

In summary, comparing the effect of the two types of nanoparticles, the addition of nano-clay to the NHL render is to be preferred to preserve the raw earth support, since it gives to the render the best mechanical compatibility with the underlying earthen masonry and the highest durability against erosion by atmospheric agents. Compatibility of materials and durability against atmospheric agents are two fundamental aspects in the protection and conservation of eco-friendly earthen building envelopes.

Since the resulting poor effect of the tested nanoparticles on the mechanical performance of plasters was quite unexpected, further studies on this topic are needed by increasing the fillers dosages and by investigating the effect of the selected nanoparticles also on the performance of clay-based coatings.

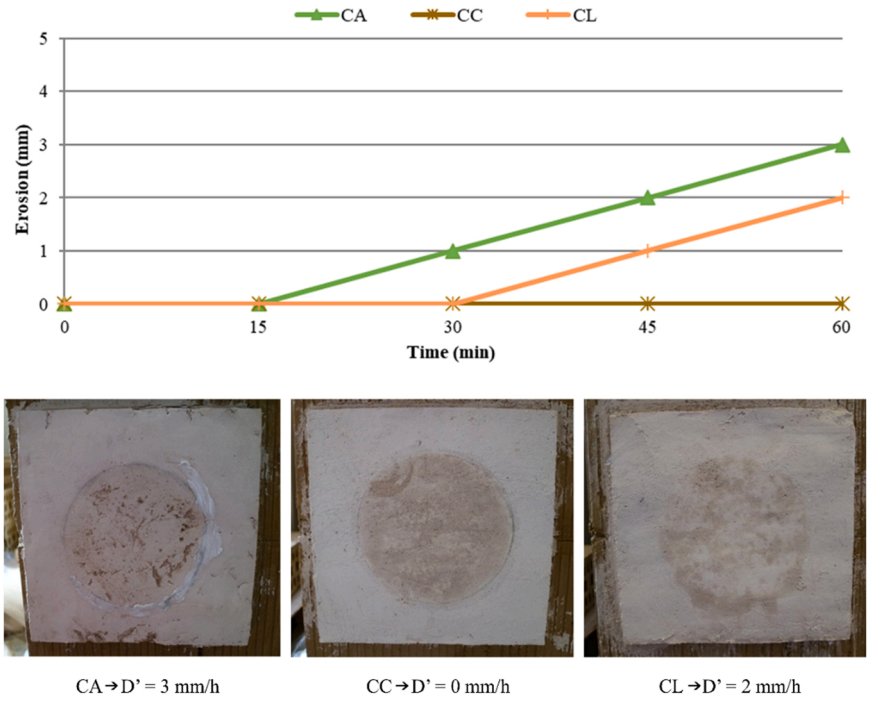

Fig. 10. Pressure spray erosion tests results.

Funding

The study was supported by Athenaeum Basic Research.

Ethical compliance

No human participants were involved in the study.

Declaration of Competing Interest

The authors declare that they have no known competing financial interests or personal relationships that could have appeared to influence the work reported in this paper.

Data availability

The data that has been used is confidential.

References

[1] K. Callebaut, J. Elsen, K. Van Balen, W. Viaene, Nineteenth century hydraulic restoration mortars in the Saint Michael's Church (Leuven, Belgium): natural hydraulic lime or cement? Cem. Concr. Res. 31 (2001) 397–403, https://doi.org/10.1016/S0008-8846(00)00499-3.
[2] A. Kalagri, I. Karatasios, V. Kilikoglou, The effect of aggregate size and type of binder on microstructure and mechanical properties of NHL mortars, Constr. Build. Mater. 53 (2014) 467–474, https://doi.org/10.1016/j.conbuildmat.2013.11.111.
[3] M. Apostolopoulou, P.G. Asteris, D.J. Armaghani, M.G. Douvika, P.B. Lourenço, L. Cavaleri, et al., Mapping and holistic design of natural hydraulic lime mortars, Cem. Concr. Res 136 (2020), https://doi.org/10.1016/j.cemconres.2020.106167.
[4] C. Sabbioni, A. Bonazza, G. Zappia, Damage of hydraulic mortars: the Venice arsenal, J. Cult. Herit. 3 (2002) 83–88, https://doi.org/10.1016/S1296-2074(02)01163-9.
[5] M. Apostolopoulou, A. Bakolas, M. Kotsainas, Mechanical and physical performance of natural hydraulic lime mortars, Constr. Build. Mater. 290 (2021), https://doi.org/10.1016/j.conbuildmat.2021.123272.
[6] B. Medvey, G. Dobszay, Durability of stabilized earthen constructions: a review, Geotech. Geol. Eng. 38 (2020) 2403–2425, https://doi.org/10.1007/s10706-020-01208-6.
[7] N. Bianco, A. Calia, G. Denotarpietro, P. Negro, Laboratory assessment of the performance of new hydraulic mortars for restoration, Procedia Chem. 8 (2013) 20–27, https://doi.org/10.1016/j.proche.2013.03.004.
[8] F. Stazi, M. Serpilli, G. Chiappini, M. Pergolini, E. Fratalocchi, S. Lenci, Experimental study of the mechanical behaviour of a new extruded earth block masonry, Constr. Build. Mater. 244 (2020), 118368, https://doi.org/10.1016/j.conbuildmat.2020.118368.
[9] M. Serpilli, F. Stazi, G. Chiappini, S. Lenci, Earthen claddings in lightweight timber framed buildings: An experimental study on the influence of fir boards sheathing and GFRP jacketing, Constr. Build. Mater. (2021), https://doi.org/10.1016/j.conbuildmat.2021.122896.

[10] D. Gulotta, S. Goidanich, C. Tedeschi, T.G. Nijland, L. Toniolo, Commercial NHL-containing mortars for the preservation of historical architecture. Part 1: compositional and mechanical characterisation, Constr. Build. Mater. 38 (2013) 31–42, https://doi.org/10.1016/j.conbuildmat.2012.08.029.
[11] P. Maravelaki-Kalaitzaki, Hydraulic lime mortars with siloxane for waterproofing historic masonry, Cem. Concr. Res. 37 (2007) 283–290, https://doi.org/10.1016/j.cemconres.2006.11.007.
[12] R. Ravi, M. Rajesh, S. Thirumalini, Mechanical and physical properties of natural additive dispersed lime, J. Build. Eng. 15 (2018) 70–77, https://doi.org/10.1016/j.jobe.2017.10.009.
[13] M. Vyšvařil, P. Bayer, Cellulose ethers as water-retaining agents in natural hydraulic lime mortars, in: Proceedings of the 13th International Conference Modern Building Materials, Structures and Techniques, MBMST 2019, 2019. ⟨https://doi.org/10.3846/mbmst.2019.014⟩.
[14] P. Maravelaki-Kalaitzaki, A. Bakolas, I. Karatasios, V. Kilikoglou, Hydraulic lime mortars for the restoration of historic masonry in Crete, Cem. Concr. Res 35 (2005) 1577–1586, https://doi.org/10.1016/j.cemconres.2004.09.001.
[15] T.S. Bozkurt, S. Yılmaz Demirkale, Investigation and development of sound absorption of plasters prepared with pumice aggregate and natural hydraulic lime binder, Appl. Acoust. (2020), https://doi.org/10.1016/j.apacoust.2020.107521.
[16] I. Torres, G. Matias, P. Faria, Natural hydraulic lime mortars - the effect of ceramic residues on physical and mechanical behaviour, J. Build. Eng. 32 (2020), https://doi.org/10.1016/j.jobe.2020.101747.
[17] M.M. Barbero-Barrera, N. Flores Medina, C. Guardia-Martín, Influence of the addition of waste graphite powder on the physical and microstructural performance of hydraulic lime pastes, Constr. Build. Mater. (2017), https://doi.org/10.1016/j.conbuildmat.2017.05.156.
[18] C. Giosuè, Q.L. Yu, M.L. Ruello, F. Tittarelli, H.J.H. Brouwers, Effect of pore structure on the performance of photocatalytic lightweight lime-based finishing mortar, Constr. Build. Mater. 171 (2018) 232–242, https://doi.org/10.1016/j.conbuildmat.2018.03.106.
[19] J. Grilo, A. Santos Silva, P. Faria, A. Gameiro, R. Veiga, A. Velosa, Mechanical and mineralogical properties of natural hydraulic lime-metakaolin mortars in different curing conditions, Constr. Build. Mater. 51 (2014) 287–294, https://doi.org/10.1016/j.conbuildmat.2013.10.045.
[20] P. Faria, P. Duarte, D. Barbosa, I. Ferreira, New composite of natural hydraulic lime mortar with graphene oxide, Constr. Build. Mater. 156 (2017) 1150–1157, https://doi.org/10.1016/j.conbuildmat.2017.09.072.
[21] K. Luo, J. Li, Z. Lu, J. Jiang, Y. Niu, Effect of nano-SiO2 on early hydration of natural hydraulic lime, Constr. Build. Mater. 216 (2019) 119–127, https://doi.org/10.1016/j.conbuildmat.2019.04.269.
[22] K. Luo, J. Li, Q. Han, Z. Lu, X. Deng, L. Hou, et al., Influence of nano-SiO2 and carbonation on the performance of natural hydraulic lime mortars, Constr. Build. Mater. 235 (2020), https://doi.org/10.1016/j.conbuildmat.2019.117411.
[23] P. Maravelaki-Kalaitzaki, Z. Agioutantis, E. Lionakis, M. Stavroulaki, V. Perdikatsis, Physico-chemical and mechanical characterization of hydraulic mortars containing nano-titania for restoration applications, Cem. Concr. Compos. 36 (2013) 33–41, https://doi.org/10.1016/j.cemconcomp.2012.07.002.
[24] A. Jerónimo, A. Camões, B. Aguiar, N. Lima, Hydraulic lime mortars with antifungal properties, Appl. Surf. Sci. 483 (2019) 1192–1198, https://doi.org/10.1016/j.apsusc.2019.03.156.
[25] F. Fernandez, S. Germinario, R. Basile, R. Montagno, K. Kapetanaki, K. Gobakis, et al., Development of eco-friendly and self-cleaning lime-pozzolan plasters for bio-construction and cultural heritage, Buildings 10 (2020) 1–12, https://doi.org/10.3390/buildings10100172.
[26] L. Rosato, M. Stefanidou, G. Milazzo, F. Fernandez, P. Livreri, N. Muratore, et al., Study and evaluation of nano-structured cellulose fibers as additive for restoration of historical mortars and plasters, Mater. Today Proc. 4 (2017) 6954–6965, https://doi.org/10.1016/j.matpr.2017.07.025.
[27] S. Kawashima, K. Wang, R.D. Ferron, J.H. Kim, N. Tregger, S. Shah, A review of the effect of nanoclays on the fresh and hardened properties of cement-based materials, Cem. Concr. Res (2021), https://doi.org/10.1016/j.cemconres.2021.106502.
[28] L. Laím, H. Caetano, A. Santiago, Review: Effects of nanoparticles in cementitious construction materials at ambient and high temperatures, J. Build. Eng. (2021), https://doi.org/10.1016/j.jobe.2020.102008.
[29] G. Lazzara, R. Fakhrullin, Nanotechnologies and Nanomaterials for Diagnostic, Conservation and Restoration of Cultural Heritage, 2018. ⟨https://doi.org/10.1016/C2017-0-00296-3⟩.
[30] J. Zhu, P. Zhang, J. Ding, Y. Dong, Y. Cao, W. Dong, et al., Nano Ca(OH)2: a review on synthesis, properties and applications, J. Cult. Herit. 50 (2021) 25–42, https://doi.org/10.1016/j.culher.2021.06.002.
[31] P.I. Girginova, C. Galacho, R. Veiga, A. Santos Silva, A. Candeias, Study of mechanical properties of alkaline earth hydroxide nanoconsolidants for lime mortars, Constr. Build. Mater. 236 (2020), https://doi.org/10.1016/j.conbuildmat.2019.117520.
[32] J. Otero, V. Starinieri, A.E. Charola, G. Taglieri, Influence of different types of solvent on the effectiveness of nanolime treatments on highly porous mortar substrates, Constr. Build. Mater. 230 (2020), https://doi.org/10.1016/j.conbuildmat.2019.117112.
[33] A.M. Forster, E.M. Szadurski, P.F.G. Banfill, Deterioration of natural hydraulic lime mortars, I: effects of chemically accelerated leaching on physical and mechanical properties of uncarbonated materials, Constr. Build. Mater. 72 (2014) 199–207, https://doi.org/10.1016/j.conbuildmat.2014.09.015.
[34] D. Gulotta, S. Goidanich, C. Tedeschi, L. Toniolo, Commercial NHL-containing mortars for the preservation of historical architecture. Part 2: Durability to salt decay, Constr. Build. Mater. 96 (2015) 198–208, https://doi.org/10.1016/j.conbuildmat.2015.08.006.
[35] EN 459-1, Building Lime Part 1: Definitions, Specifications and Conformity Criteria, 2015.
[36] CEN, EN 1015-12:2000, Methods of Test for Mortar for Masonry – Part 12: Determination of Adhesive Strength of Hardened Rendering and Plastering Mortars on Substrates, 8523, 2000, p.10.
[37] E. Hamard, J.C. Morel, F. Salgado, A. Marcom, N. Meunier, A procedure to assess the suitability of plaster to protect vernacular earthen architecture, J. Cult. Herit. 14 (2013) 109–115, https://doi.org/10.1016/j.culher.2012.04.005.
[38] F. Stazi, A. Nacci, F. Tittarelli, E. Pasqualini, P. Munafò, An experimental study on earth plasters for earthen building protection: the effects of different admixtures and surface treatments, J. Cult. Herit. 17 (2016) 27–41, https://doi.org/10.1016/j.culher.2015.07.009.
[39] E.W. Washburn, The dynamics of capillary flow, Phys. Rev. (1921), https://doi.org/10.1103/PhysRev.17.273.
[40] UNI EN 12504-4:2005, Testing Concrete – Part 4: Determination of Ultrasonic Pulse Velocity, 2005.
[41] CEN 1999, EN 1015-11: methods of test for mortar for masonry - part 11: determination of flexural and compressive strength of hardened mortar, Eur. Comm. Stand. 12 (1999).
[42] UNI EN 998-1:2016, Specification for Mortar for Masonry - Part 1: Rendering and Plastering Mortar, n.d.
[43] CEN, Conservation of Cultural Heritage – Test Methods – Measurement of Water Absorption by Pipe Method, EN 163022013, 2013.
[44] D. Vandevoorde, M. Pamplona, O. Schalm, Y. Vanhellemont, V. Cnudde, E. Verhaeven, Contact sponge method: Performance of a promising tool for measuring the initial water absorption, J. Cult. Herit. (2009), https://doi.org/10.1016/j.culher.2008.10.002.
[45] UNI EN 12664:2002, Thermal Performance of Building Materials and Products – Determination of Thermal Resistance by Means of Guarded Hot Plate and Heat Flow Meter Methods – Dry and Moist Products of Medium and Low Thermal Resistance, n.d.
[46] New Zealand Standard, NZS 4298, Materials and Workmanship for Earth Buildings – Appendix D, Erosion Test, Pressure Spray Method, 2020.
[47] N. Farzadnia, A.A. Abang Ali, R. Demirboga, M.P. Anwar, Effect of halloysite nanoclay on mechanical properties, thermal behavior and microstructure of cement mortars, Cem. Concr. Res. (2013), https://doi.org/10.1016/j.cemconres.2013.03.005.
[48] H. Lindgreen, M. Geiker, H. Krøyer, N. Springer, J. Skibsted, Microstructure engineering of Portland cement pastes and mortars through addition of ultrafine layer silicates, Cem. Concr. Compos. (2008), https://doi.org/10.1016/j.cemconcomp.2008.05.003.
[49] J. Vera-Agullo, V. Chozas-Ligero, D. Portillo-Rico, M.J. García-Casas, A. Gutiérrez-Martínez, J.M. Mieres-Royo, et al., Mortar and concrete reinforced with nanomaterials, Nanotechnol. Constr. 3 (2009), https://doi.org/10.1007/978-3-642-00980-8_52.
[50] H. Moosberg-Bustnes, B. Lagerblad, E. Forssberg, The function of fillers in concrete, Mater. Struct. 37 (2004) 74–81, https://doi.org/10.1617/13694.
[51] E. Berodier, K. Scrivener, Understanding the filler effect on the nucleation and growth of C-S-H, J. Am. Ceram. Soc. 97 (2014) 3764–3773, https://doi.org/10.1111/jace.13177.
[52] G. Choudalakis, A.D. Gotsis, Permeability of polymer/clay nanocomposites: a review, Eur. Polym. J. 45 (2009) 967–984, https://doi.org/10.1016/j.eurpolymj.2009.01.027.

[53] H. Kim, Y. Miura, C.W. MacOsko, Graphene/polyurethane nanocomposites for improved gas barrier and electrical conductivity, Chem. Mater. 22 (2010) 3441–3450, https://doi.org/10.1021/cm100477v.
[54] I.-M. Low, A. Hakamy, F. Shaikh. Hemp Fabric Reinforced Organoclay–Cement Nanocomposites: Microstructures, Physical, Mechanical and Thermal Properties, 2017, pp. 19–36, https://doi.org/10.1007/978-3-319-56588-0_3.
[55] S. Khandelwal, K.Y. Rhee, Evaluation of pozzolanic activity, heterogeneous nucleation, and microstructure of cement composites with modified bentonite clays, Constr. Build. Mater. (2022), https://doi.org/10.1016/j.conbuildmat.2022.126617.
[56] J. Jiang, L. Hou, Z. Lu, J. Li, J. Wang, Y. Yang, et al., Pore structure optimization and hardened performance enhancement of nanopore-rich lightweight cement paste by nanosilica in swelled bentonite, Appl. Nanosci. (2020), https://doi.org/10.1007/s13204-019-01155-6.
[57] F. Stazi, M. Serpilli, G. Chiappini, M. Pergolini, E. Fratalocchi, S. Lenci, Experimental study of the mechanical behaviour of a new extruded earth block masonry, Constr. Build. Mater. 244 (2020), 118368, https://doi.org/10.1016/j.conbuildmat.2020.118368.
[58] M.R. Irshidat, M.H. Al-Saleh, Influence of nanoclay on the properties and morphology of cement mortar, KSCE J. Civ. Eng. 22 (2018) 4056–4063, https://doi.org/10.1007/s12205-018-1642-x.
[59] J. Thamboo, N. Jayarathne, A. Bandara, Characterisation and mix specification of commonly used masonry mortars, SN Appl. Sci. 1 (2019) 1–12, https://doi.org/10.1007/s42452-019-0312-z.
[60] C.D. Udawattha, G.A.H.H. Galkanda, R.U. Halwatura, A study on natural rain surface erosion of different walling materials in tropics, in: Proceedings of the MERCon 2018 – 4th International Multidisciplinary Moratuwa Engineering Research Conference, 2018, pp. 84–89. ⟨https://doi.org/10.1109/MERCon.2018.8421938⟩.